Improved Covariance Matrix Estimation in Spectrally Inhomogeneous Sea Clutter with Application to Adaptive Small Boat Detection

P. L. Herselman, H. J. de Wind

CSIR Defence, Peace, Safety and Security
Pretoria, SOUTH AFRICA
{pherselman,rdewind}@csir.co.za

Abstract— Asymptotically optimal coherent detection techniques yield sub-clutter visibility in heavy-tailed sea clutter. The adaptive linear quadratic detector inherently assumes spectral homogeneity for the reference window of the covariance matrix estimator. This paper investigates the validity of this assumption on real data that have been recorded with a medium resolution X-band radar. Proving empirically that this basic assumption is the exception rather than the rule, the effects of spectral inhomogeneity are investigated. Various improvements to the current estimator and detector are suggested and evaluated. This is specifically applied to the detection of small rigid inflatable boats, with empirical results presented for a range of boat manoeuvres. A specific example highlights the vulnerability of the chosen detector to self-masking.

I. INTRODUCTION

Detection of small boats (sub $15\ m$) in heavy seas has become a critical function for maritime surveillance radar [1], especially the Rigid Inflatable Boat (RIB) class with lengths as short as 4.2 m. This class of boat has a very small Radar Cross Section (RCS) (typically less than $10\ m^2$) and it is generally accepted that a detector with sub-clutter visibility is required for operation in all sea conditions at appreciable distances. Frequency agility has been used effectively to increase the Signal-to-Interference Ratio (SIR) by a factor of approximately $\sqrt{n}$ [2],[3]. Coherent adaptive detection techniques have been investigated recently with theoretical results suggesting significant sub-clutter visibility [4],[5],[6],[7]. Amongst these the Adaptive Linear-Quadratic (ALQ) detector has received particular interest as an Asymptotically Optimal Detector (AOD). The basic principle of this class of detectors is that the sea clutter is parsed through a whitening filter before being subjected to a Generalized Likelihood Ratio Test (GLRT). A prerequisite for the whitening filter is an accurate estimate of the sea clutter covariance matrix $\mathbf{M}$, which is often estimated from a target free region around the test cell. It is inherently assumed that the random processes of the reference cells are independent and identically distributed (*i.i.d.*). Empirical evidence suggests that this is rather the exception than the rule [1], especially in an up/down-wind configuration with gusty winds or whenever the wind starts causing whitecaps.

The research presented in this paper is focused on proving empirically that sea clutter has to be characterised as being spectrally inhomogeneous in general and that the assumption that the sea clutter processes of different range cells are *i.i.d.* are only valid in certain conditions, *e.g.* at long ranges and for cross-swell geometries. The empirical analysis have been performed on data recorded with an experimental, monopulse, X-band radar with vertical polarization as depicted in Fig. 1.

The effects of the incorrect assumption of *i.i.d.* processes are investigated, with specific attention to the inability of the detector to whiten the interference completely. Under the initial assumption, it should be possible to set a theoretical threshold for Constant False Alarm Rate (CFAR) operation [6]. It is proven in this paper that this is not the case and that is necessary to set the threshold χ_t as a function of the steering vector Doppler f_d. Improvements to the estimation technique are suggested and evaluated where a more localised $\mathbf{M}$ is estimated using either frequency agility or the immediate time history of a limited number of closely spaced range gates, where the latter is only possible in a radar with adaptive dwell times. Improved whitening is observed with the subsequent convergence of the actual threshold to the theoretical threshold for a given probability of false alarm P_{FA}.

Detection performance is evaluated on empirical data for the standard Range Acting (RA) ALQ detector with a fixed as well as Doppler-dependant threshold, proving improved detectability for the latter case. Performance is evaluated for a range of boat manoeuvres and a specific example will highlight the vulnerability of the ALQ detector to self-masking.

Fig. 1.   Radar deployed on Signal Hill with open view of sea

The layout of the paper is as follows: In the next session the basic principles of the ALQ detector will be discussed together with experimental results from the OTB 2006 measurement trial, highlighting its inability to completely whiten interference that is spectrally inhomogeneous. Section III presents an overview of the second measurement trial of which the recorded data have been analysed and produced most of the empirical results presented in this paper. Section IV performs an in-depth analysis on the whitening achieved by the ALQ detector and the effects thereof on P_{FA} and $\chi_t(f_d)$. Section V evaluates the improvement of the probability of detection P_d on recorded data of a 4.2 m pencilduck (a specific type of RIB). Section VI investigates potential improvements to the estimation algorithm together with empirical results for different sea conditions, suggesting significant improvements in interference whitening and detector sensitivity.

II. ALQ DETECTOR OVERVIEW

It is possible to represent the sea clutter random process by the class of Spherically Invariant Random Processes (SIRP's). A random vector (representative of a burst in a pulsed radar system) obtained by sampling a SIRP is a Spherically Invariant Random Vector (SIRV) whose Probability Density Function (PDF) can be completely described by the mean vector, the covariance matrix $\mathbf{M}$ as well as the first-order PDF [6]. This multivariate compound-Gaussian model permits flexible modelling of the pulse-to-pulse correlation properties of sea clutter as well as the local power, which in itself is a random process often modelled as a Gamma process.

It is possible to design an AOD by extending the GLRT approach, as suggested by Kelly [4] for Gaussian interference, to the SIRP model for non-Gaussian interference. Assume that the radar transmits a coherent train of m pulses. The associated m received complex samples can be constructed as a vector $\mathbf{z} = [z(1) \dots z(m)]^T$. Under the assumption that $\mathbf{M}$ is known exactly, the ALQ detector can be expressed mathematically as

$$\frac{|\mathbf{p}^H \mathbf{M}^{-1} \mathbf{z}|^2}{(\mathbf{p}^H \mathbf{M}^{-1} \mathbf{p})(\mathbf{z}^H \mathbf{M}^{-1} \mathbf{z})} \underset{H0}{\overset{H1}{\gtrless}} \chi_t \ , \qquad (1)$$

where $\mathbf{p}$ is the steering vector typically constructed with elements $p_i = e^{j2\pi i f_d T}$ [5], T the radar PRI and f_d the target Doppler frequency [6]. It is generally accepted that $\mathbf{M}$ is highly dependent on the radar configuration, geometry and the environmental conditions and has to be estimated from adjacent range gates that are not contaminated by the boat itself. Various estimation techniques have been proposed [8]. Gini and Greco [6] describe one such technique that makes a good compromise between detection losses and hardware processing requirements,

$$\hat{\mathbf{M}}_{AML}(i+1) = \frac{1}{K} \sum_{k=1}^{K} \frac{m \cdot \mathbf{z}_k \mathbf{z}_k^H}{\mathbf{z}_k^H \hat{\mathbf{M}}_{AML}(i)^{-1} \mathbf{z}_k} \qquad (2)$$

for $i = 0, 1, 2, \dots, N_{it}$, where $\mathbf{z_k}$, $k = 1 \dots K$ are the secondary data vectors from the K reference cells. During each iteration the Approximately Maximum Likelihood (AML) estimation is normalized such that its trace is equal to

m. Since the ALQ detector involves inversion of $\mathbf{M}$, care has to be taken to ensure that the matrix doesn't become singular. This can be ensured by setting the number of independent sea clutter time vectors at different range gates k equal to at least the length of the test vector m, $k \geq m$ [4]. Detectability can be improved by increasing this ratio, but at the expense of increased hardware processing requirements.

The ALQ detector was evaluated on real sea clutter data recorded with the Fynmeet C- to X-band pulsed CW RCS measurement facility [1], with a 5.7 m RIB steering away from the radar into the oncoming waves and prevailing wind. The estimator have been configured with $m = 15$, $k = 30$ and $N_{it} = 3$. The latter is sufficient under most sea clutter conditions [6]. The high-resolution spectrogram in Fig. 2(a) of the range bin containing the boat clearly highlights the spectral inhomogeneity of sea clutter under certain conditions. Fig. 2(b) demonstrates the general whitening of the interference, the inability to whiten the interference when the local spectrum deviates significantly from the average sea clutter spectrum as well as the slight spreading of the boat Doppler response. Of particular concern is the breakthrough of the sea clutter at certain Doppler frequencies. For CFAR operation this will require an increase in the threshold χ_t, which will be investigated in depth in Section IV.
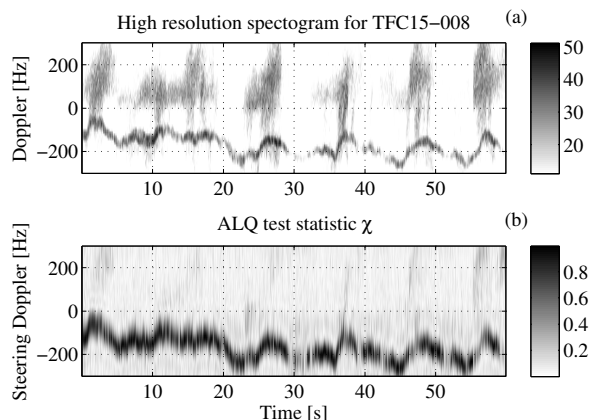

Fig. 2. ALQ whitening evaluated on real sea clutter and 5.7 m RIB data: (a) High-resolution spectrogram, (b) Test statistic

III. MEASUREMENT TRIAL SUMMARY

The experimental X-band monopulse radar (Fig. 1) was deployed on Signal Hill close to Cape Town, South Africa at location $33°55'15.62''S$, $18°23'53.76''E$, 294 m above mean sea level, as indicated on the plan view in Fig. 3. The shortest distance to the coast line was 1250 m at a bearing of $288°N$. The site provided $140°$ azimuth coverage from $240°N$ to $20°N$, of which a large sector spanned open sea whilst the remainder looked towards the West Coast coastline from the direction of the open sea. The radar had an open view of Robben Island at a distance of 11 km. Grazing angles ranging from $10°$ at the coastline to $0.3°$ at the radar instrumented range of 60 km were obtained.
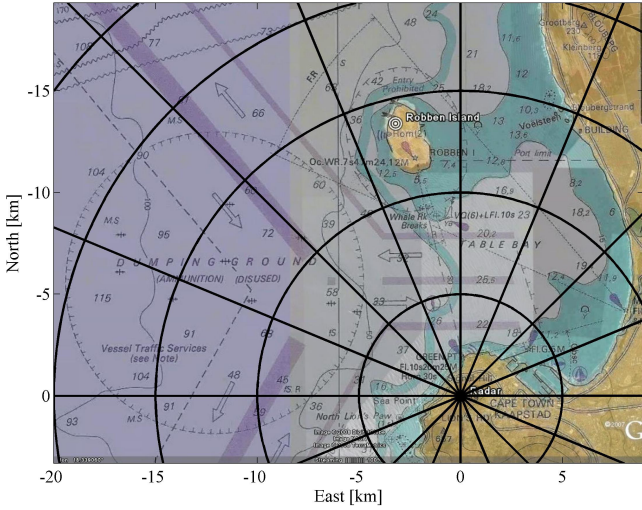
Fig. 3.   Plan overview of radar deployment site

Fig. 4.   Spectrogram for spectrally homogeneous sea clutter

Fig. 5.   Spectrogram for spectrally inhomogeneous sea clutter

Sea clutter datasets were recorded on eight different days over a period of thirteen days, while datasets of instrumented boats were recorded on five different days. In addition datasets were recorded for a large variety of non-cooperative boats of opportunity. Recordings were made using a range of fixed frequency and stepped frequency waveforms. Local wind conditions were measured at the radar, Robben Island, Cape Town Harbour as well as Slangkop (south-southwest of the radar). The predominant wind direction was northwestern, but with southeastern intervals. The average wind speed varied between $0\ kts$ and $40\ kts$, with a maximum gust of $60\ kts$. The local wave conditions were measured with a seabed-based wave sensor at Camp's Bay and a directional wave buoy at Cape Point and numerically modelled at eight other locations in Table Bay and around Robben Island. The significant wave height ranged between 1 and 4.5 m, whilst the swell direction varied between $230\,^\circ N$ and $270\,^\circ N$. The tracks of the intstrumented boats were estimated using a differential-processing Global Positioning System (GPS) receiver.

IV. INTERFERENCE WHITENING IN SPECTRALLY HOMOGENEOUS SEA CLUTTER

This section sets out to performs an in-depth analysis on the degree of whitening obtained by the ALQ detector with the estimator as described by Gini and Greco [6] and the effects thereof on P_{FA} and $\chi_t(f_d)$. Two datasets from the Signal Hill 2007 measurement trial have been identified that best represent the different cases of spectral homogeneity and inhomogeneity, hereafter referred to as datasets 1 and 2 respectively. The spectrograms for these datasets are plotted in Fig. 4 and Fig. 5 for a single range cell. These are complimented with plots of the second normalised intensity moment NIM_2 as a function of frequency, calculated as

$$NIM_2(f_d) = E\{z(f_d)^2\}/E^2\{z(f_d)\}\ , \qquad (3)$$

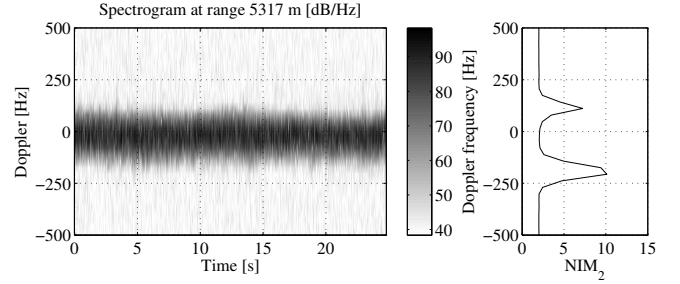where $z(f_d)$ is the power spectral density at f_d. This is often used to quantify the Rayleigh-likeness of the envelope random process [9]. Theoretically, $NIM_2 = 2$ for a random process with Rayleigh envelope statistics. Values higher than 2 is indicative of increased spikiness at the specific Doppler frequency. In both datasets it is clear that $NIM_2 \approx 2$ at the Doppler frequencies where there were only thermal noise. At the edges of the sea clutter Doppler spectrum NIM_2 rises due to the spikiness at these frequencies. A clear distinction between datasets 1 and 2 is that NIM_2 for dataset 2 was severely raised at the positive Doppler frequencies, those frequencies characterised by bursts of wide Doppler bandwidth scattering caused by wind gusts and/or whitecaps at the crests of the waves. These plots suggest that the Range Acting (RA) estimator may yield a very accurate $\mathbf{M}_{AML}$ for dataset 1, but a poor localised estimate for dataset 2.
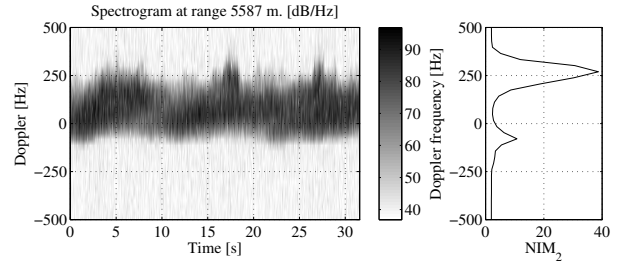
The test statistic χ was calculated for both datasets with $m = 15$, $k = 30$ and $N_{it} = 3$. At each Doppler frequency (steering Doppler) P_{FA} was calculated as a function of the threshold χ_t and the results plotted in Fig. 6 and Fig. 7, together with the mean and fixed threshold. For dataset 1 the different curves are closely spaced with only slight variations in the χ_t for a fixed P_{FA}. However, for dataset 2 there are certain Doppler frequencies that requires a significantly higher χ_t, especially at low levels of P_{FA}, e.g. 10^{-4}. Consequently a larger χ_t is required for a fixed threshold compared to the mean threshold over all Doppler frequencies. It is very difficult to set χ_t theoretically for a given P_{FA} and it has to be set based on the local interference, *e.g.* using an adaptive algorithm that may be based on the estimation of $NIM_2(f_d)$ locally. Fig. 8 plots $\chi_t(f_d)$ and from this it can be deduced that there is strong correlation between high levels of NIM_2 and a high χ_t. However, there is evidence that such an adaptive algorithm may need additional estimates, since the clutter

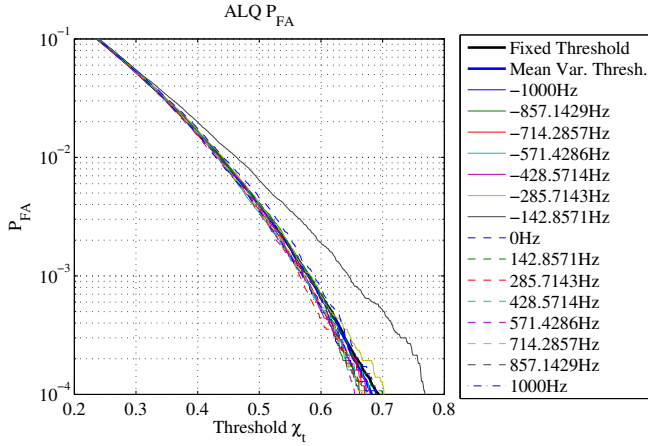spectral edge opposite to the bursts have a raised NIM_2 whilst χ_t can be set relatively low.

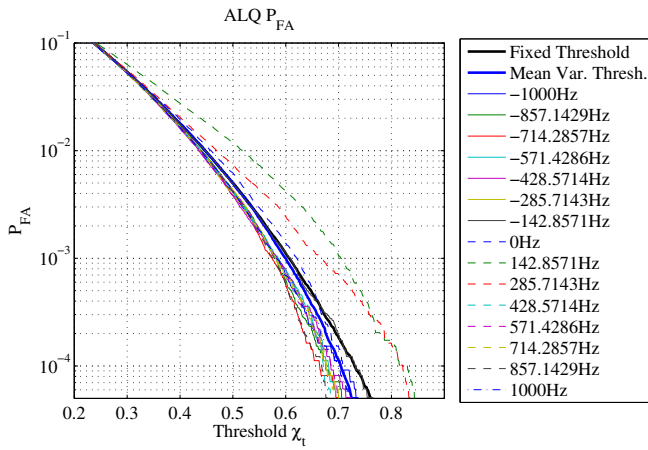Fig. 6. Probability of false alarm as function of χ_t for dataset 1

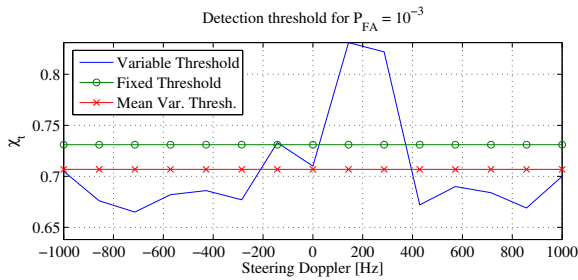Fig. 7. Probability of false alarm as function of χ_t for dataset 2

Fig. 8. Detection threshold as a function of Steering Doppler, f_d

From this analysis it is clear that under certain conditions the standard RA ALQ detector [6] effectively whitens the sea clutter allowing AOD with a threshold that can be set theoretically. On the other hand, especially in spectrally inhomogeneous sea clutter, the RA ALQ detector performs poorly at whitening the sea clutter yielding a significantly raised χ_t for the same P_{FA} that can't be set theoretically and has to be estimated

from the data itself. With a Doppler-dependent $\chi_t(f_d)$, the average threshold is significantly lower than a fixed threshold, which should lead to improved detectability of small boats. This is investigated in-depth in section V. However, Doppler-dependant thresholding still requires adaptive setting of the threshold.

V. DOPPLER-DEPENDENT ALQ DETECTION

This section evaluates the improvement of P_d for RA ALQ Doppler-dependent thresholding on recorded data of a 4.2 m pencilduck, with a mean mean RCS of $\hat{\sigma}_0 \approx 1\ m^2$. In the first dataset evaluated the boat was floating close the southwestern shore of Robben Island. The local wave height was $3\ m$ with the local wind $6\ kts\ NE$. The radar look angle was $343\ °N$ at range $R = 11\ km$ with grazing angle $\theta = 1.5\ °$. The signal-to-clutter ratio and the clutter-to-noise ratio were $6\ dB$ and $24\ dB$ respectively. Fig. 9 plots a high resolution spectrogram of the range cell containing the boat.
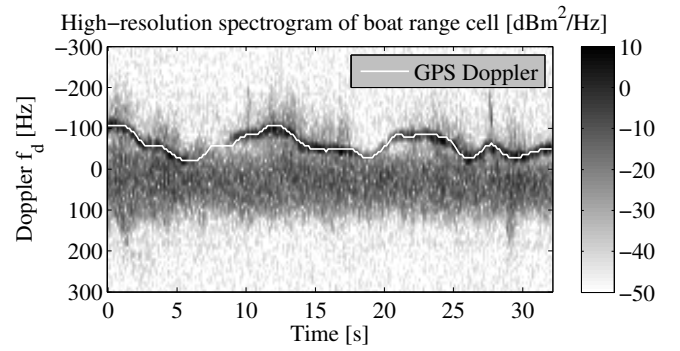

Fig. 9. Spectrogram of range cell containing pencilduck

Fig. 10(a) plots the spectrogram with a dwell time equal to that of the ALQ detector. Fig. 10(b) plots the test statistic with the Doppler-dependent thresholding detections overlaid at $P_{FA} = 10^{-4}$. Fig. 10(c) plots the sliding window P_d for both Doppler-dependent and fixed thresholding with window lenght $L = 31$. The ability of the detector to whiten the sea clutter is clear in Fig. 10(b), whilst the boat signature show very little evidence of decorrelation. An improvement from 19% to 23% in $E\{P_d\}$ is observed. For such a low SIR this is rather significant. The fading in target signature and the subsequent fading in detectability may very well be due to shadowing of the boat by the seawaves.

In the second dataset the pencilduck was racing at a speed of $40\ kts$ radially outbound at a range of $21.5\ km$. The high resolution spectrogram (Fig. 11) reveals that the racing boat caused a signicant local disturbance of the sea water (e.g. splashing waves and water spray by the propeller), decreasing the localised SIR to less than $-10\ dB$. Overlaying detections on the range-time intensity plot revealed very intermitend detection of the boat, where it can be clearly distinguised from the surrounding background. In fact, it is the localised disturbance that were distinguised with the eye. In addition, steady detections were made on a flock of birds flying radially inbound with a RCS about $10\ dB$ lower than the boat.
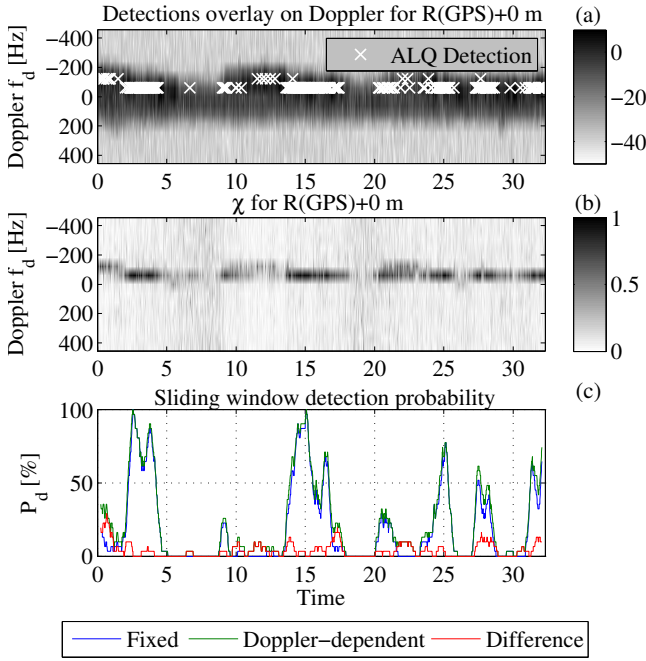
Fig. 10. Performance of Doppler-dependent thresholding

Fig. 12 plots χ for the range bin containing the boat. The sea clutter and localised disturbance are whitened over all Doppler, effectively masking the boat. In this case the RA ALQ can't be classified as an AOD, since a range-Doppler cell-averaging CFAR detector can be configured to steadily detect the boat due to the seperation in Doppler of the interference and the boat signature and its narrow Doppler spectrum.
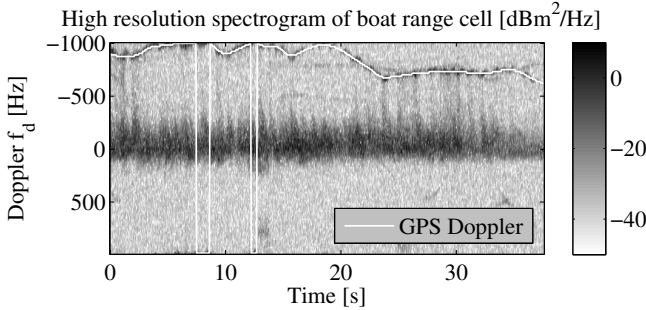

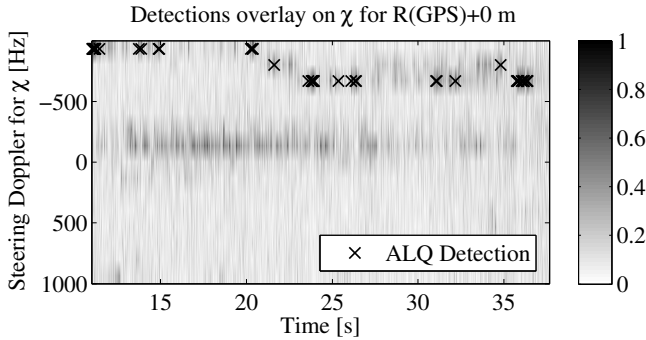Fig. 11. High resolution spectogram of fast moving pencilduck

Fig. 12. ALQ masking of fast moving pencilduck

VI. IMPROVED M ESTIMATION IN SPECTRALLY HOMOGENEOUS SEA CLUTTER

It is postulated that detectability can be improved by a more localised estimation of **M**. This requires a large number k of sea clutter time vectors yielding uncorrelated sample vectors of the localized speckle. These sample vectors should have a Doppler spectrum (and autocorrelation) that is representative of the local sea at the test cell that is not contaminated by boat reflectivity. The latter is typically obtained by the insertion of guard cells. Average sea wave lengths for sea states 3 to 5 range from $25\ m$ to $85\ m$ in open sea conditions [2]. With whitecaps typically localised to the crests of waves, the localised sample vectors have to be collected as closely spaced to the test cell as possible. With medium resolution radar (typical $\Delta R \approx 15\ m$) it is not feasible to collect sample vectors at roughly the same phase of the sea wave, especially in the presence of guard cells. With higher resolution ($\Delta R \leq 1.5\ m$) it becomes feasible to insert a guard length of 7.5 m (optimized for RIB's) and still have range cells that have similar Doppler characteristics to the test cell. However, with high values of m it remains difficult for the RA ALQ detector. Two methods are proposed in the following subsections aimed at yielding a large number of sample vectors k at the immediate range cells adjacent to the guard cells.

A. Frequency Agile ALQ

Sea clutter decorrelates with frequency agility when the frequency step size exceeds the pulse bandwidth, $\Delta f_c \geq B$ [2]. Independent sample vectors can be obtained by transmitting a burst of stepped frequency pulses with $\Delta f_c \geq B$ and a burst rate yielding unambiguous Doppler. $k/2$ sample vectors are constructed by sampling m pulses at each frequency at each of the two range cells adjacent to the guard cells. This requires a burst length $BLEN = m$. Due to range ambiguity and transmitter PRF constraints, it was set to $BLEN \leq 7$ in the empirical analysis of the method. No guard cells were used to ensure that the Doppler characteristics of the sample vectors best resembles that of the test vector, which is acceptable for data containing only sea clutter. The resultant $\chi_t(f_d)$ are plotted for both RA and Frequency Agile (FA) estimators in Fig. 13.
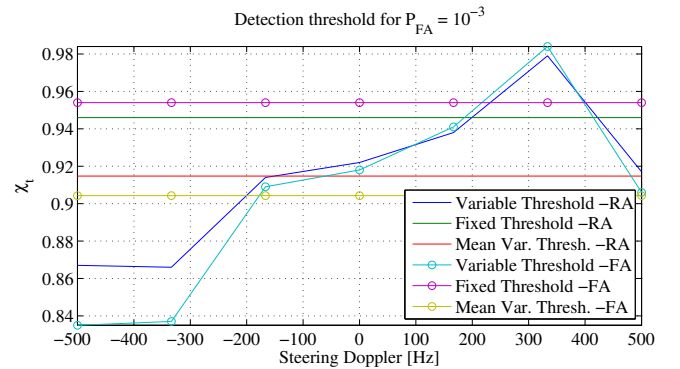

Fig. 13. Detection threshold as a function of Steering Doppler, f_d

As can be expected for lower m, the threshold has increased for both estimators, but the general trend can be observed that on average a lower threshold can be set for the FA estimator compared to the RA estimator. In certain cases little difference was observed. However, the general trend suggest that this is a promising method that has to be investigated further for higher values of m, requiring a larger number of unique frequencies and/or higher range resolution.

B. Time Acting ALQ

Sea clutter decorrelates after 5 to 20 ms [10]. With adaptive dwell times (*e.g.* phase array or staring beam radar) a number of independent sample vectors can be obtained at the same range gate over a time interval during which the sea clutter spectrum doesn't vary significantly, typically in the order of hundreds of milliseconds. $k/2$ independent, consecutive sample vectors are constructed at each of the two range cells adjacent to the guard cells. In a high resolution radar this can be extended to include multiple range cells, thus increasing k and subsequently P_d. Analyses were perfomed, omitting the guard cells, with $m = 15$, $k = 30$ and $N_{it} = 3$. The resultant $\chi_t(f_d)$ is plotted for both RA and Time Acting (TA) estimators in Fig. 14 and Fig. 15 for datasets 1 and 2 respectively.
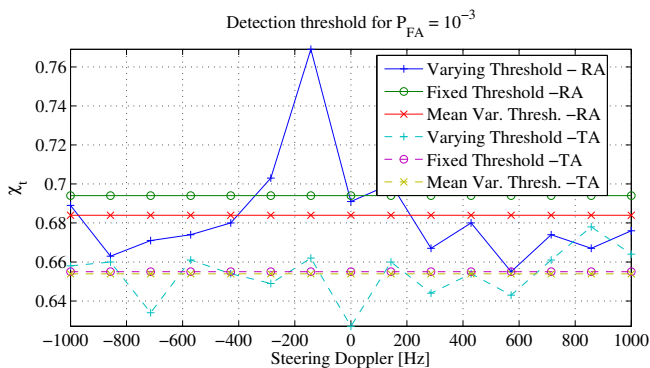

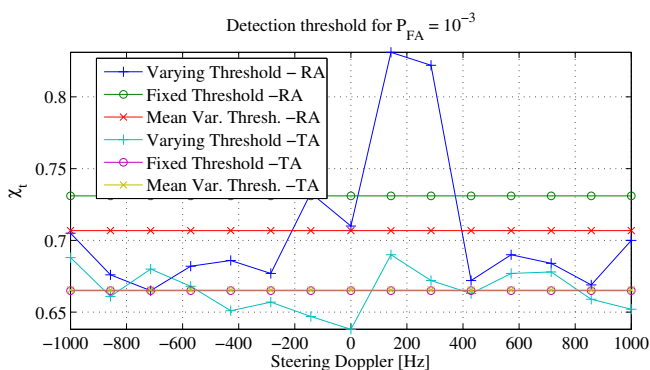Fig. 14. Detection threshold as a function of steering Doppler, for dataset 1

Fig. 15. Detection threshold as a function of steering Doppler, for dataset 2

It is clear that χ_t can be reduced for the TA ALQ, which should yield an improved P_d. In addition, the mean and fixed thresholds are similar, enabling χ_t to be set theoretically,

rather than adaptively. In dataset 2 there are signs of a raised threshold that correlates with the high threshold levels for the RA ALQ detector. This suggests that the sample vectors are not fully representative of the test vector. It is important to further evaluate this estimation method on higher resolution data, in which case it will be possible to also evaluate P_d for real boat data.

VII. CONCLUSIONS

In this paper, it was shown that improved detection performance can be obtained for the RA ALQ detector by Doppler-dependent thresholding, especially in spectrally inhomogeneous sea clutter. However, it still requires adaptive thresholding, due to the inability of the ALQ to perfectly whiten the interference. Improved whitening and detectability can be realised by a more localised estimation of $\mathbf{M}$. Two methods were proposed and evaluated. Empirical results clearly indicates improved performance, but this will have to be complemented with higher range resolution data to confirm improved detectability and to allow the insertion of guard cells that are required in a practical system.

It was shown using real data that the ALQ can under certain conditions be subject to self-masking. A definite contribution to the knowledgebase is the importance of not only modelling the sea clutter and boat reflectivity accurately, but also to model the local disturbance caused by small boats, especially during fast manoeuvring.

REFERENCES

[1] P. L. Herselman and C. J. Baker, "Analysis of calibrated sea clutter and boat reflectivity data at c- and x-band in south african coastal waters," in *RADAR 2007*, 2007.

[2] F. E. Nathanson, *Radar Design Principles: Signal Processing and the Environment*. Mendham NJ: SciTech Publishing, Inc., 1999.

[3] K. D. Ward, R. J. A. Tough, and S. Watts, *Sea Clutter: Scattering, the K Distribution and Radar Performance*, ser. IET Radar, Sonar and Navigation Series. London: IET, 2006, no. 20.

[4] E. Kelly, "An adaptive detection algorithm," *Aerospace and Electronic Systems, IEEE Transactions on*, vol. AES-22, no. 2, pp. 115–127, 1986.

[5] F. Gini, "Sub-optimum coherent radar detection in a mixture of k-distributed and gaussian clutter," *Radar, Sonar and Navigation, IEE Proceedings -*, vol. 144, no. 1, pp. 39–48, 1997.

[6] F. Gini and M. Greco, "Covariance matrix estimation for cfar detection in correlated heavy tailed clutter," *Signal Processing*, vol. 82, no. 12, pp. 1847–1859, Dec. 2002.

[7] M. McDonald and S. Lycett, "Fast versus slow scan radar operation for coherent small target detection in sea clutter," *Radar, Sonar and Navigation, IEE Proceedings -*, vol. 152, no. 6, pp. 429–435, 2005.

[8] F. Gini, "Performance analysis of two structured covariance matrix estimators in compound-gaussian clutter," *Signal Processing*, vol. 80, no. 2, pp. 365–371, Feb. 2000.

[9] C. J. Baker, "Spectral properties of radar sea clutter," in *IEE Colloquium on Radar Clutter and Multipath Propagation*, vol. 11, 1989, pp. 1–6.

[10] A. Farina, F. Gini, M. Greco, and L. Verrazzani, "High resolution sea clutter data: statistical analysis of recorded live data," *IEE proc., Radar sonar navig.*, vol. 144, no. 3, pp. 121–130, June 1997.